metals

MDPI

Article

Dendritic Segregation of Zn-Al Eutectoid Alloys

Ildiko Peter [1,*], Mirela Agapie [2] and Bela Varga [2]

[1] Department of Applied Science and Technology, Institute of Science and Engineering of Materials for the Innovative technologies, Politecnico di Torino, Corso Duca degli Abruzzi 24, 10129 Torino, Italy

[2] Department of Materials Science, Transilvania University of Brasov, B-dul Eroilor 29, 500036 Brasov, Romania; agapiemirela18@gmail.com (M.A.); varga.b@unitbv.ro (B.V.)

* Correspondence: ildiko.peter@polito.it; Tel.: +39-011-090-4670

Received: 10 October 2018; Accepted: 6 November 2018; Published: 8 November 2018

Abstract: The structural investigations performed and described in this paper are focused on both the segregation phenomenon at the dendrite level, and on the external structure in the equilibrium state. Qualitative and quantitative investigations of the Zn-Al eutectoid alloy (22% Al) structures in equilibrium and non-equilibrium states were considered and studied, revealing that, in this composition, dendritic segregation determines the eutectic transformation. Solidification in non-equilibrium conditions controls both the eutectic transformation and the significant variation of the chemical composition within the dendritic unit, as well as in other constituents. The most important effect of dendritic segregation is on the ratio of the different phases and on their geometry and distribution within the metallic matrix, which determines the material topology. The phenomena involved in such conditions are governed by the structural transformations, which take place during solidification and cooling in a solid state.

Keywords: Zn-Al alloys; eutectoid; segregation; β-phase

1. Introduction

Distinctiveness, antifriction capability, corrosion resistance and technological properties, mainly relating to their excellent castability and cutting machinability, make Zn-Al alloys a promising material for industrial applications, for which most of this composition is currently employed [1–9]. The superplastic properties of alloys with eutectoid composition contribute to making these alloys an interesting target for investigations relating to their structural transformations [10–13].

With the introduction of Zn-Al alloys with increased Al content, the dendritic segregation phenomenon occurs as a peculiarity of single phase Al-Zn alloys [14]. The dimensional stability of Zn-Al alloys is significantly influenced by dendritic segregation and decreases over time. In Al-Zn systems the diffusion of the alloying elements takes place at a low velocity. This determines the significant structural modifications, compared to those in the equilibrium structure, like the presence of the eutectic transformation in the alloy with 40% (wt%) of Al [14].

At the same time, investigations concerning Zn–Al alloys with an Al content that is higher than the concentration corresponding to the eutectic point are difficult because of the lack of common opinion on the thermal equilibrium phase diagram. It is important to note that in regard to the Zn-Al system, until the first part of the 20th century, various forms of the phase diagrams [15–17] have been proposed. The research performed in the last 20–30 years, however, considers only two of the phase diagram options [17–19].

The most important differences between the two diagrams relate to the absence/presence of the peritectic transformation at 443 °C and to the lack/existence of the β-phase at high temperatures.

For the structural analysis of this research paper the phase diagram proposed by Presnyakov has been chosen, according to [18,19].

The many-sided structural transformations of Zn-Al alloys with increased Al content processed in different conditions have been determined and are still a topic of great interest in the scientific community [20–24].

Solidification in non-equilibrium conditions, at the velocity usually used for the casting of Zn-Al alloys, determines, for one, a difference in the chemical compositions of a wide range of the dendrite segment and, for another, the appearance of non-equilibrium constituents. The structural analysis was performed by optical and scanning electron microscopy (OM, Nikon-Omnimet-Buehler, SEM, Leo 1450VP, Zeiss, Ramsey, NJ, United States) and the distribution of the elements was verified by energy-dispersive X-ray spectrometry (EDS, Oxford Microprobe, Zeiss, Ramsey, NJ, United States). Differential scanning calorimetry (MAIA 200F3, Netzsch-Gerätebau Gmbh, Selb, Germany) and dilatometric measurements (LINSEIS, L75/230, DIL-Linseis Messgeräte Gmbh, Selb, Germany) were used to complete the study.

2. Experimental Section

Table 1 reports the chemical composition of the binary Zn–Al alloy investigated in this research paper.

Table 1. Chemical composition (wt%) of the Zn–Al alloy investigated.

Alloy	Chemical Composition (wt%)							
ZnAl22	Al 21.85	Cu 0.195	Mg 0.002	Cd 0.006	Pb 0.002	Fe 0.117	Sn 0.0009	Zn 77.82

An electric furnace with SiC resistance and graphite crucibles was used to develop the alloy. Gravity casting was performed and the effects of the solidification conditions were evaluated using dies made up of: (i) steel (OL, dimension $14 \times 80 \times 160$ mm^3), (ii) refractory ceramic (C, $\Phi 40 \times 50$ mm^2) and (iii) refractory ceramic cooled in the furnace (CC, $\Phi 40 \times 50$ mm^2). The registered cooling curves were used to determine the transformation temperatures and the cooling rate (Table 2).

Table 2. Cooling rate and transformation temperatures as indicated by the registered cooling curves.

Casting Conditions	Cooling Rate (°C/min) and Transformation Temperatures (°C)		
	Beginning of Solidification	Eutectic Transformation	Eutectoid Transformation
OL	1080 (456)	2160 (396)	240 (259)
C	38.4 (484)	14.4 (381)	6 (250; 252)
CC	12 (486.5)	7.8 (382.7)	4.8 (254; 257)

The samples for the structural and thermal analyses have been extracted from semi-fabricated castings and, simultaneously, samples cast with steel die, of the size indicated in Figure 1a, were extracted and submitted to thermal treatment (hardening) using a specific ad-hoc tool projected and realized for this research. The schematic illustration of this device is reported in Figure 1b and the parameters of the thermal treatment process are illustrated in the diagram reported in Figure 1c.

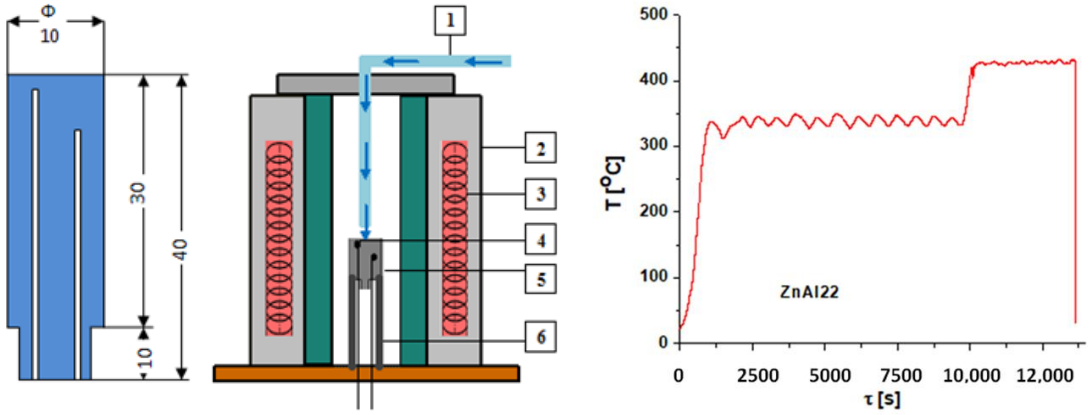

(**a**) (**b**) (**c**)

Figure 1. Set-up of the tool used for thermal treatment: (**a**) shape and dimensions of the samples submitted to thermal treatment; (**b**) device used for the thermal treatment: 1—cooling system using water; 2—furnace; 3—electrical resistance; 4—thermocouple; 5—sample; 6—sample holder; (**c**) thermal treatment parameters.

3. Results and Discussion

Figure 2 reports the microstructures obtained in the different casting conditions. Figure 3 reports the EDS results obtained along a line. The yellow line indicates where the analysis has been performed (along a line), the red line shows the Al concentration and the blue line relates to the Cu concentration. The bottom of Figure 3 shows the variation of the Al concentration of the ZnAl22 alloy cast with steel die as a function of distance (l, expressed in μm).

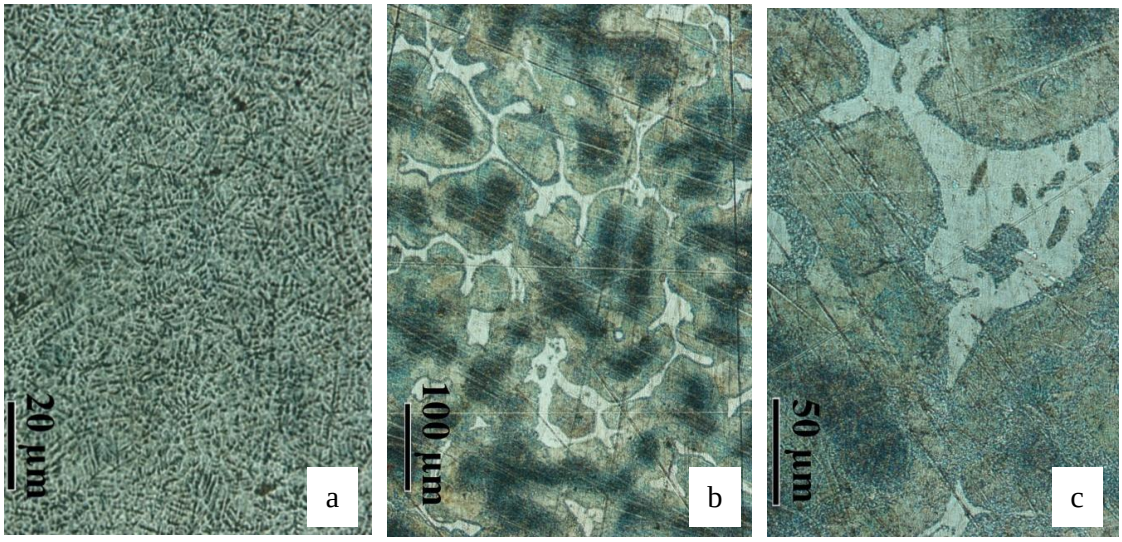

Figure 2. Optical Microstructures for the ZnAl22 alloy cast in: (**a**) steel die; (**b**) ceramic refractory die; (**c**) ceramic refractory die cooled in the furnace.

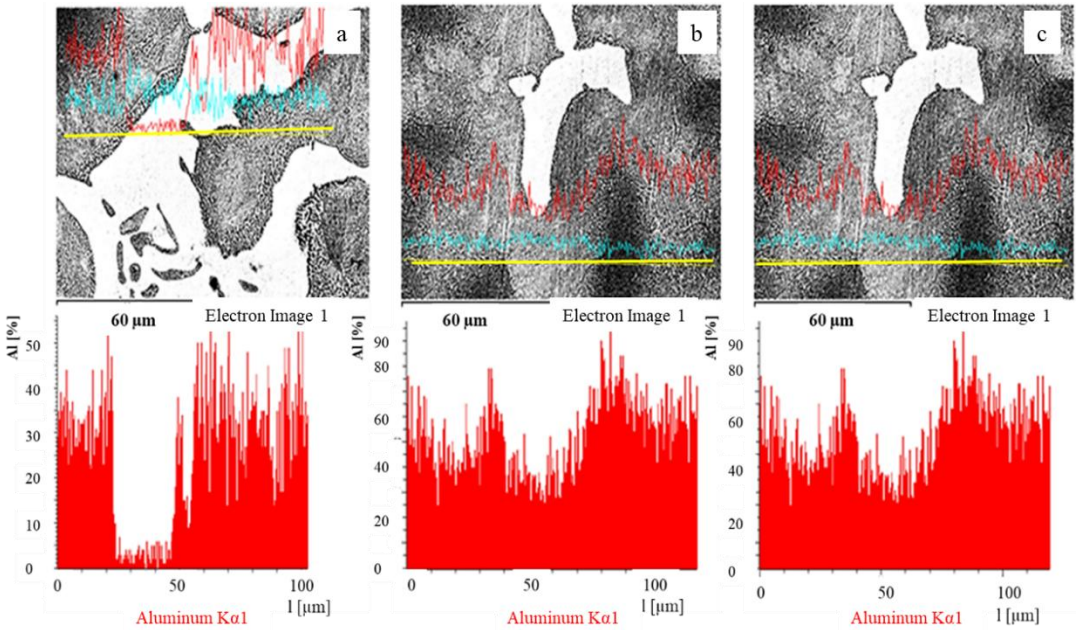

Figure 3. EDS analysis results and the variation of the concentration of the Al in the ZnAl22 alloy cast with steel die for three (**a**–**c**) different areas.

For the ZnAl22 alloy cast with steel die, the structural particularities have been illustrated in Figure 4a–c, while Table 3 reports the values of the concentrations obtained for the points indicated in Figure 4.

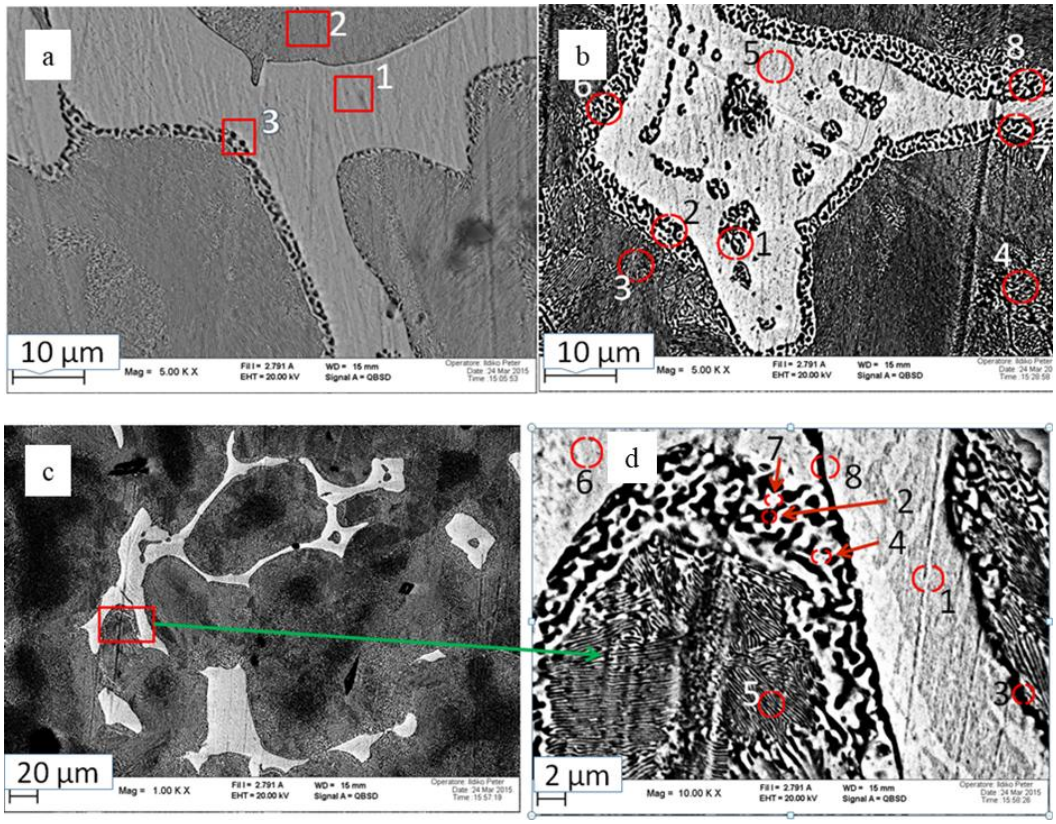

Figure 4. Indication of the different (**a**–**d**) areas for the ZnAl22 alloy cast with steel die.

Table 3. Composition of the areas indicated in Figure 5.

Analyzed Area		Alloying Elements Concentration (wt%)		Phase/Constituent
Figure	Analyzed Point	Zn	Al	
(**a**)	1	65	35	eutectic
	2	62	38	s.s.α intermediate layer
	3	62.5	37.5	s.s.α superficial layer
(**b**)	1	55	45	eutectoid from eutectic
	2	64	36	s.s.α superficial layer
	3	45	55	s.s.α intermediate layer
	4	43	57	s.s.α central area
	5	45	55	eutectic
	6	46	54	s.s.α superficial layer
	7	47	53	s.s.α superficial layer
	8	46.5	53.5	s.s.α superficial layer
(**c**)	1	92	8	eutectic
	2	35	65	s.s.α superficial layer
	3	52	48	s.s.α superficial layer
	4	55	45	s.s.α superficial layer
	5	55	45	s.s.α intermediate layer
	6	94	6	eutectic
	7	64	36	s.s.α superficial layer
	8	52	48	s.s.α superficial layer

The EDS analysis results for the thermal treated ZnAl22 alloy in the biphasic zone (S + L) are reported in Figure 5, where the same annotation of Figure 3 has been used for the analysis of the composition along a line. The lamellar shaped eutectoid phases can be seen when the alloy is cast with steel die. The thickness of the eutectoid phase is lower than 0.5–0.2 μm. The geometry and the size of this phase vary as a function of the conditions related to the development of the β-phase and are developed as a primary phase or following the eutectic reaction. The microstructural observations and the compositional analysis on micro-areas and along a line have shown that the concentration of the alloying element (Al) varies in a widely in both the solid solution α (s.s.α) and in the eutectic one. At the dendrite level, different structural regions can be observed with significant morphological differences. In the centre of dendrites of the s.s.α the concentration of Al is at its highest, reaching levels of 80–90%. In the central area, the appearance of a nearly concentric region can be observed with significant extension, whereas a characteristic of the eutectoid transformation is the appearance of the fine lamellar phase. On the surface of the dendrites there is a layer with quasi-uniform thickness, made up of two phases with polygonal shape, where the Al concentration is at about 50%. In the eutectic phase (eutectoid) of the interdendritic space, the Al concentration is minimal, 5–8%, which is close to the concentration which corresponds to the eutectic point in the thermal equilibrium phase diagram.

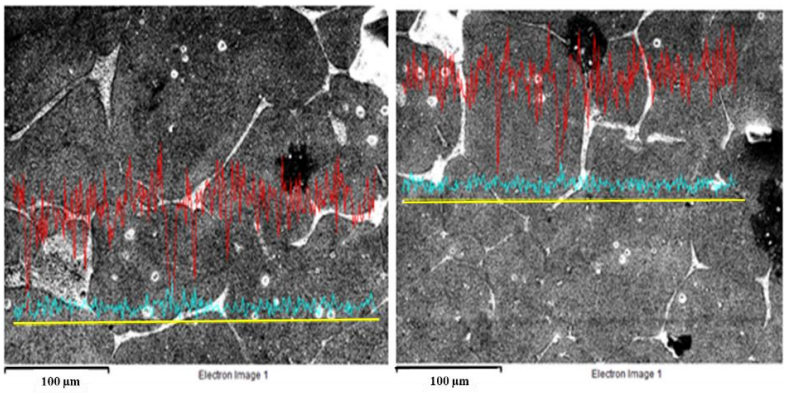

(**a**) (**b**)

Figure 5. EDS analysis for the ZnAl22 alloy (thermal treated condition) in the biphasic zone (S + L) for two (**a**–**b**) different areas.

It was discovered that the structure is homogeneous; on the section of the β crystals the Al concentration was not significantly varied (between 22.37% and 27.14%) and they were superior (3–4%) to the average concentration of Al in the alloy. In the interdendritic regions (in the eutectic) the Al concentration was lower than the average concentration of Al in the alloy.

The investigations focused on analysis of the stability of the β-phase, a metastable phase, in different thermal treatment conditions. Therefore, by reheating the thermal treated sample up to 400 °C with a holding time of 10 min and a cooling rate of 5 °C/min, the decomposition of the metastable structure was inevitable with the development of the phases (Figure 6a), according to the phase diagram.

The main particularities of the developed structure consist of a specific arrangement (like a rosette) of the eutectoid phase. When the heating temperature is above liquidus temperature (500 °C) and the cooling rate is 10 °C/min and again the development of the dendritic structure arises (Figure 6b).

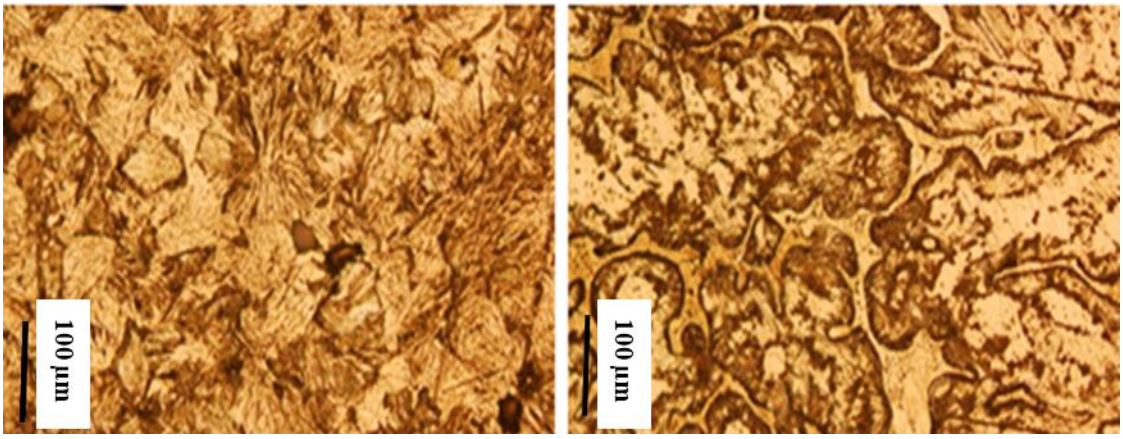

(**a**) (**b**)

Figure 6. The alloy structure after the annealing performed during: (**a**) Dilatometric (DIL) and (**b**) Differential Scanning Calorimetry (DSC) analysis.

It is very important to mention that, contrary to some scientific literature [25–27], the monophasic structure developed only from the β-phase and shows higher stability at room temperature, a stability which continues for some years (about four years).

Since the eutectic and eutectoid transformations play an important role in the development of the final structure, DSC and DIL analyses have been carried out to obtain some information concerning the transformation. This was done using small samples extracted from the castings obtained in different conditions. The heating/cooling of the samples was performed two times at different rates (5, 10 and 20 °C/min); first on the casted samples and second during the repetition of the DSC analysis on the same sample).

Analyzing the DSC curves (Figure 7), the parameters related to the phase transformations were evaluated, and, in particular, the temperature and transformation energy were considered. The DSC results are reported in Table 4 (there is a simplification of the data acquired during the analysis, where a total of 18 pairs of DSC heating/cooling curves were registered).

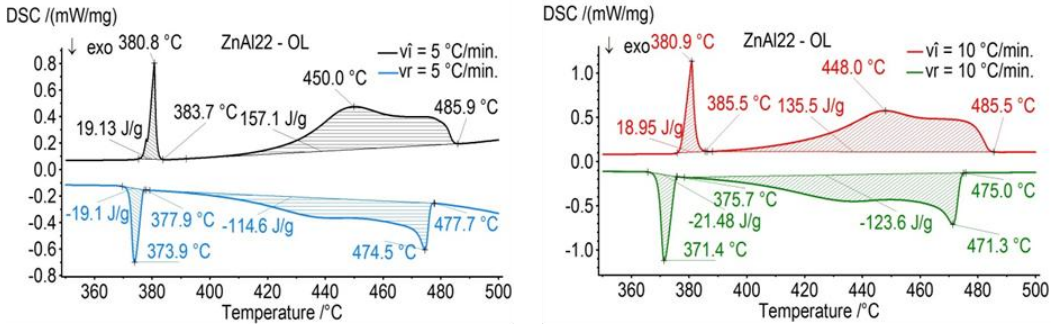

Figure 7. DSC curves for the ZnAl22 alloy cast with steel die with: (**a**) vî = vr = 5 °C/min and (**b**) vî = vr = 10 °C/min.

The data obtained were analyzed in order to demonstrate how the casting and processing conditions and the heating/cooling during DSC analysis (the first heating/cooling step can be considered as thermal treatment) influence the phase transformations. This is relevant in Zn–Al alloys with eutectoid composition.

The first find was on the samples analyzed with DSC; the liquidus temperature registered during cooling (solidification) was 10–20 °C lower than that registered during heating (melting).

During cooling, the overcooling phenomenon was revealed, for both the eutectic and for the eutectoid transformations (Figure 8).

Table 4. Summary of the DSC analysis results.

Sample Code	$v_{\hat{i}}/v_r$ (°C/min)	Heating					
		$P_{1\hat{i}}$		$P_{2\hat{i}}$		$P_{3\hat{i}}$	
		$T_{eud\text{-}\hat{i}}$ (°C)	$Q_{eud\text{-}\hat{i}}$ (J/g)	$T_{eut\text{-}\hat{i}}$ (°C)	$Q_{eud\text{-}\hat{i}}$ (J/g)	$T_{l\text{-}i}$ (°C)	$Q_{\alpha\text{-}\hat{i}}$ (J/g)
OL-I	5	284.2	21.7	378.6	0.2514	487.3	152.3
C-II		282.7	24.29	381.8	14.83	487.3	134.6
C-I		284.8	31.29	382.2	16.15	491.9	186.4
C-II		282.5	31.45	381.4	17.01	490.3	186.5
CC-I		283.2	33.13	380.2	11.11	490.5	200.8
CC-II		282.1	30.94	380.8	15.39	492.1	189.3
		Cooling					
		$P_{1\hat{i}}$		$P_{2\hat{i}}$		$P_{3\hat{i}}$	
		$T_{l\text{-}r}$ (°C)	$Q_{\alpha\text{-}r}$ (J/g)	$T_{eut\text{-}r}$ (°C)	$Q_{eut\text{-}r}$ (J/g)	$T_{eud\text{-}r}$ (°C)	$Q_{eud\text{-}r}$ (J/g)
OL-I	10	471.3	−123.6	371.4	−21.48	239.2	−24.16
OL-II		471.3	−123.3	371.6	−21.46	239.4	−24.24
C-I		474.0	−136.9	369.4	−19.32	237.7	−27.09
C-II		473.8	−137.2	368.7	−19.46	238.1	−27.25
CC-I		470.9	−126.5	369.7	−20.05	238.0	−26.28
CC-II		470.5	−127.1	369.8	−20.18	238.1	−25.76

Observation: Meaning of the symbols used in the table: P_1, P_2 and P_3 signify the eutectoid (eud), eutectic (eut) and liquidus (s.s.α) transformation temperatures, T_l–lichidus signifies temperature and Q-phase signifies heat transformation. The second index "î" is related to the transformations which are produced during heating, while "r" is related to those which are formed during cooling.

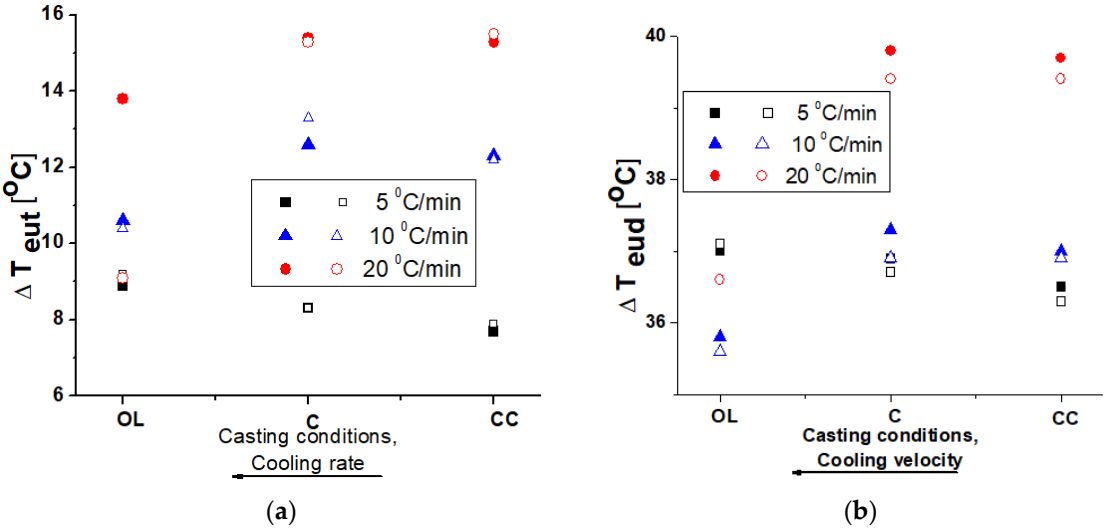

Figure 8. Variation of the degree of overcooling as a function of the casting conditions. (**a**) at the eutectic transformation; (**b**) at the eutectoid transformation.

Please note that in Figures 8 and 9 the filled markers (square, triangle, circle) indicate the values related to the first round of heating/cooling, while the un-filled markers refer to the second cycle of heating/cooling in the DSC device. The samples cooled inside the DSC furnace, in all cases, show the same behavior concerning the relationship between the cooling rate and the overcooling grade of the phase transformations (eutectic and eutectoid, respectively). Overcooling for the transformation in solid state (eutectoid) is higher than that observed for the eutectic transformation and the eutectoid transformation temperature is affected only slightly by the cooling rate applied during solidification compared to the eutectic transformation temperature.

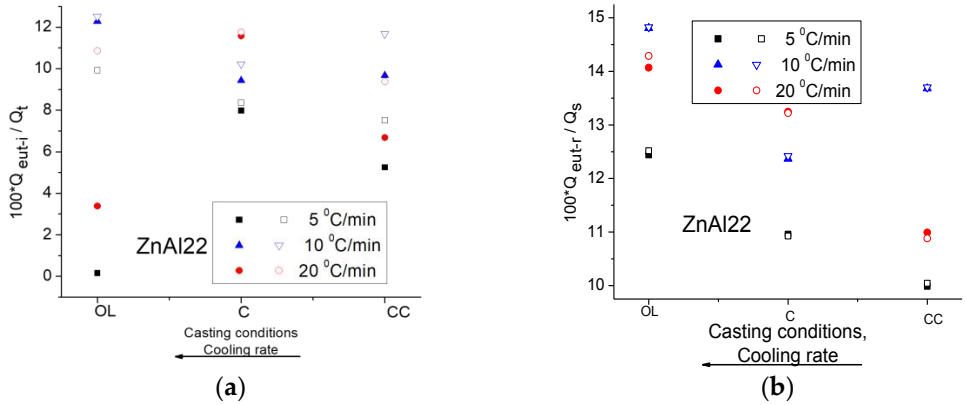

Figure 9. Ratio of the eutectic heat transformation of the total heat required for the state of aggregation: (**a**) during heating and (**b**) during cooling.

For analysis of the thermal energy related to the phase transformations one has to consider the various relationships between different quantities, like latent heat of fusion (Q_t), which represents the heat related to the inverse eutectic transformation, and the heat associated with the melting of the solid solution ($Q_{\alpha-\hat{i}}$). Similarly, the latent heat of solidification (Q_s) is created from the heat necessary for the solidification of the solid solution ($Q_{\alpha-r}$) and related to the eutectic transformation ($Q_{eut-\hat{i}}$). In this context, the following relations hold true:

$$Q_t = Q_{eut-\hat{i}} + Q_{\alpha-\hat{i}} \quad (1)$$

$$Q_s = Q_{\alpha\text{-r}} + Q_{\text{eut-r}} \quad (2)$$

$$Q_t = -Q_s \quad (3)$$

The heat required for the eutectic transformation of the aggregation state, for both heating and cooling, is reported in Figure 10. An increase in the cooling rate during casting determines an improvement in the ratio of the eutectic transformation energy of the total melting energy and of the solidification energy, respectively. The ratio of this value is higher in the case of solidification.

The first observation relates to the energy ratio (heat) which corresponds to the inverse eutectic transformation of the total heat necessary for melting. This is about 8–12%, a ratio determined on the basis of the structural analysis [28]. This value of the eutectic ratio was considered as a starting point for the configuration of the phase diagram modified within the range of the concentration that corresponds to the eutectic and eutectoid points [28]. It is important to note that during cooling, the ratio of the eutectic transformation (11–14%) shows higher values than those registered during heating.

The energy related to the eutectoid transformation is about twofold higher than the eutectic transformation energy and it represents about 18% of the total melting heat required. Moreover, it can also be considered a function of the fraction of the constituents that make up the alloy. Therefore, for the cooling rate encountered in the case of gravity casting of the alloy in different dies (steel and two types of refractory materials), as well as in heating/cooling conditions of the samples submitted to DSC measurements (for a wide range of cooling rate), the development of about the same quantity of eutectic is observed.

The eutectoid transformation has been investigated by DIL analysis as well. For this analysis, samples have been heated and maintained in the monophasic domain, at 420 °C for 6 min, in order to obtain a homogenized structure. At the holding temperature the structure consists only of the β-phase.

Cooling has been performed in two ways: The first is controlled while the second occurs in an un-controlled way. For the controlled cooling and for the three cooling velocities considered, the contraction curves have been reported in Figure 10.

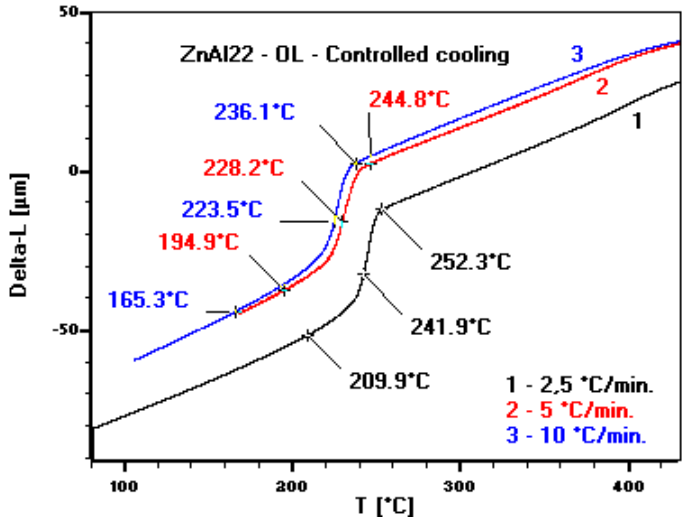

Figure 10. Contraction curves registered for the alloy produced by gravity cast with steel die during controlled cooling.

On these curves, the beginning and the end of the transformation, as well as the temperature when the transformation occurs with the maximum velocity (the peak on the derivative of the contraction curve), have been indicated.

Figure 11 reports the cooling curves in the case of free cooling in the DIL apparatus.

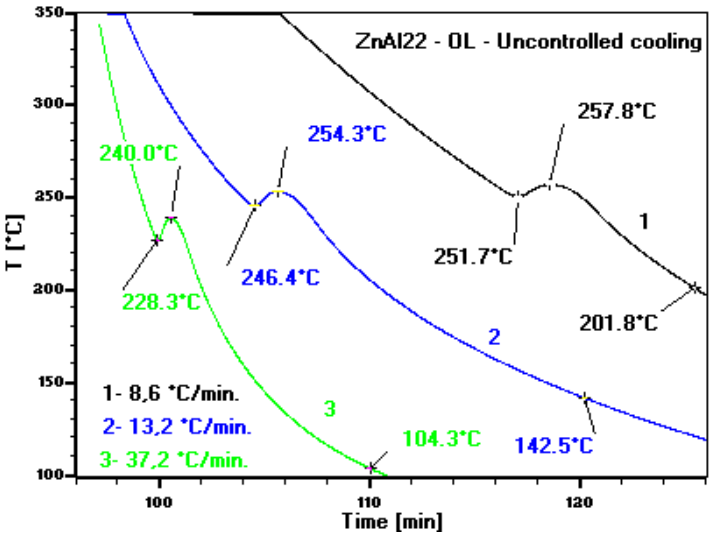

Figure 11. Cooling curves registered during DIL analysis, when the cooling was un-controlled for the gravity casted alloy and using steel die.

For the curves reported in Figure 11, the cooling rates have been analytically calculated for the range before the transformation temperature. These curves give evidence of both the over-cooling phenomenon for the eutectoid transformation and the phenomenon related to the recoalescence of the alloy (Table 5 and Figure 12).

Table 5. Degree of overcooling and the recoalescence phenomenon registered for the different cooling rates.

Alloy	Processing Condition	v_r (°C/min)	T_{eud} (°C)	ΔT_{eud} (°C)	$T_{reheating}$ (°C)	$\Delta T_{reheating}$ (°C)
ZnAl22	OL	0.0	275.0	0	0.0	-
		8.6	251.7	23.3	257.8	6.1
		13.2	246.4	28.6	254.3	7.9
		37.2	228.3	46.7	240.0	11.7

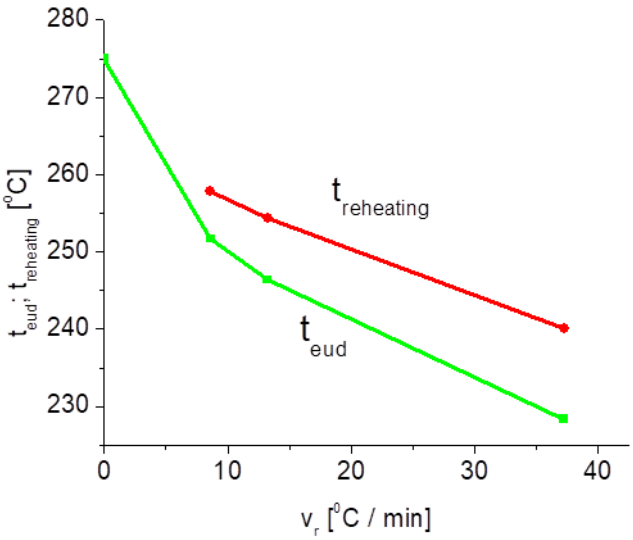

Figure 12. Variation of the eutectoid and recoalescence transformation temperatures as a function of the un-controlled cooling rate applied during DIL analysis for the gravity casted ZnAl22 alloy (in steel die).

As reported in Figure 12, as in the case of the eutectoid transformation, an increase in the cooling rate determines an increase in the overcooling grade and in the re-heating temperature during the

recoalescence phenomenon. When the sub-cooling rate increases, the finest microstructure is obtained. The variation of overcooling for the eutectoid transformation in the controlled and un-controlled mode is reported in Figure 13 and it is possible to observe that the eutectoid transformation during controlled cooling takes place at lower temperatures than in the case of free cooling.

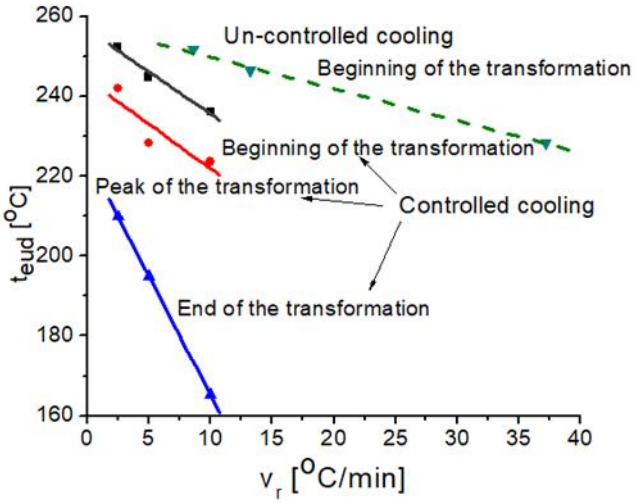

Figure 13. The registered overcooling in the eutectoid transformation via the controlled and un-controlled method during DIL analysis.

4. Conclusions

The research carried out has revealed that the investigated alloy solidification (the usual cooling rate during the casting of these alloys) determines, in non-equilibrium state, a pronounced segregation of Al at the level of the dendrites and the presence of the eutectic transformation. The most important effect of dendritic segregation is on the variation of the ratio of different phases and constituents with respect to the values indicated by the thermal phase diagram, as well as their form, geometry and fineness within the metallic matrix. The conditions leading to the decomposition of the phases during the eutectic and eutectoid transformation, when a hard segregation of Al occurs at the level of the dendrites, determine the structural modifications of the alloy.

The structural and thermal analysis results determine the fraction of the eutectic at about 10% in the structure of the ZnAl22 alloy with eutectoid composition. The dendritic segregation for this composition is accentuated, finding areas in the alloy's structure where the Al concentration reaches 90%. The β-phase obtained during thermal treatment (hardening) in the biphasic zone (L + S) does not show any segregation phenomenon. The monophasic structure, developed only from the β-phase, shows stability for more than four years, contrary to some literature data.

During cooling, the registered ratio of heat, related to the eutectic transformation (11–14%) from the whole quantity of heat necessary for the phase transformation (liquid → solid), represents a higher level than the one obtained during heating. Eutectoid overcooling is about three times higher than that of eutectic. Eutectoid overcooling, in the case of un-controlled cooling, is lower than the one obtained during controlled cooling. In the case of non-controlled cooling of the samples, a higher cooling rate resulted in a more accentuated difference between the eutectoid transformation temperature and the recoalescence temperature.

Author Contributions: Conceptualization, B.V., Methodology, B.V., M.A., I.P., Analysis and investigations, MA., I.P., Data Curation, M.A., Supervision, B.V., Writing-Original Draft Preparation, M.A., B.V., Writing-Review & Editing, B.V., I.P.

Acknowledgments: M. Agapie and B. Varga wish to acknowledge the Structural Founds Project, Sectoral Operational Programme Human Resources Development, ID137516 and the Structural Founds Project PRO-DD (POS-CCE, O.2.2.1., ID 123, SMIS 2637, ctr. No 11/2009) financed by the European Social Fund and by the Romanian Government, respectively, for providing the infrastructure used in this research work.

Conflicts of Interest: The authors declare no conflicts of interest.

References

1. Babić, M.; Ninković, R. Zn–Al alloys as tribomaterials. *Tribol. Ind.* **2004**, *26*, 3–7.
2. Babić, M.; Ninković, R.; Rac, A.; Batajnica, R. Sliding wear behavior of Zn–Al alloys in conditions of boundary lubrication. *Citeseer* **2005**, 60–64.
3. Babić, M.; Ninković, R.; Mitrović, S.; Bobić, I. Influence of heat treatment on tribological behavior of Zn–Al alloys. *Tribol. Ind.* **2007**, *29*, 22–31.
4. Babić, M.; Mitrović, S.; Ninković, R. Tribological potencial of zinc-aluminium alloys improvement. *Tribol. Ind.* **2009**, *31*, 15–28.
5. Babić, M.; Mitrović, S.; Jeremic, B. The influence of heat treatment on the sliding wear behavior of a ZA-27 alloy. *Tribol. Int.* **2010**, *43*, 16–21. [CrossRef]
6. Babic, M.; Slobodan, M.; Džunic, D.; Jeremic, B.; Ilija, B. Tribological behavior of composites based on ZA-27 alloy reinforced with graphite particles. *Tribol. Lett.* **2010**, *37*, 401–410. [CrossRef]
7. Elzanaty, H. The effect of different copper content on microstructure and mechanical properties of Zn-40Al and Al-40Zn alloys. *Int. J. Res. Eng. Technol.* **2014**, *2*, 55–62.
8. Krajewski, W.K.; Zak, P.L.; Orava, J.; Greer, A.; Krajewski, P.K. Structural stability of the high-aluminium zinc alloys modified with Ti addition. *Arch. Foundry Eng.* **2012**, *12*, 61–66. [CrossRef]
9. Krajewski, W.K.; Greer, A.; Krajewski, P.K. Trends in the development of high-aluminium zinc alloys of stable structure and properties. *Arch. Metall. Mater.* **2013**, *58*, 845–847. [CrossRef]
10. Zhu, Y.H.; Chan, K.C.; Pang, G.K.H.; Yue, T.M.; Lee, W.B. Structural Changes of α Phase in Furnace Cooled Eutectoid Zn–Al Based Alloy. *J. Mater. Sci. Technol.* **2007**, *23*, 347–352.
11. Zyska, A.; Konopka, Z.; Łagiewka, M.; Nadolski, M.; Chojnacki, A. High-aluminium zinc alloy (ZnAl27Cu2) modified with titanium and boron. *Arch. Foundry Eng.* **2009**, *9*, 237–240.
12. Ling, F.W.; Laughlin, D.E. The kinetics of transformation in Zn–Al superplastic alloys. *Metall. Trans. A* **1979**, *10*, 921–928. [CrossRef]
13. Zhang, Z.M.; Wang, J.C.; Yang, G.C.; Zhou, Y.H. Microstructural evolution of the supersaturated ZA27 alloy and its damping capacities. *J. Mater. Sci.* **2000**, *35*, 3383–3388.
14. Krupkowski, A.; Pawlovski, A.; Dukiet-Zawadzka, B. Dendritic segregation of Al-Zn alloys solidifying at different velocity. *Arch. Hutn.* **1969**, *14*, 295–301.
15. Broniewski, M.M.W.; Kucharski, J.; Winawer, W. Sur la structure des alliages aluminium-zinc. *Rev. Met. Paris* **1937**, *34*, 449–461. [CrossRef]
16. Isihara, T. On the equilibrium diagram of the aluminium-zinc system. *J. Inst. Met.* **1925**, *33*, 73–90.
17. Mondolfo, L.F. Equilibrium diagrams in non-ferrous alloys. *Appl. Phase Diagr. Metall. Ceram.* **1978**, *2*, 1382–1408.
18. Zhu, Y.H. General Rule of Phase Decomposition in Zn–Al Based Alloys (II)—On Effects of External Stresses on Phase Transformation. *Mater. Trans.* **2004**, *45*, 3083–3097. [CrossRef]
19. Torres-Villasenor, G.; Martínez-Flores, E. Hybrid Materials Based on Zn–Al Alloys. In *Metal, Ceramic and Polymeric Composites for Various Uses*; Cuppoletti, J., Ed.; IntechOpen: London, UK, 2011; p. 684.
20. Zhu, Y.H. Phase transformations of eutectoid Zn–Al alloys. *Asian J. Mater. Sci.* **2001**, *36*, 3973–3980. [CrossRef]
21. Dorantes-Rosales, H.J.; López-Hirata, V.M.; Méndez-Velázquez, J.L.; Saucedo-Munõz, M.L.; Hernández-Silva, D. Microstructure characterization of phase transformations in a Zn-22 wt% Al-2 wt% Cu alloy by XRD, SEM, TEM and FIM. *J. Alloys Compd.* **2000**, *313*, 154–160. [CrossRef]
22. Dorantes-Rosales, H.J.; López-Hirata, V.M.; Esquivel-González, R.; González-Velazquez, J.L.; Moreno-Palmerin, J.; Torres Castillo, A. Zn-22Al-2Cu alloy phase transformations at different homogenizing temperatures. *Met. Mater. Int.* **2012**, *18*, 385–390. [CrossRef]
23. Dorantes-Rosales, H.J.; López-Hirata, V.M.; Moreno-Palmerin, J.; Cayetano-Castro, N.; Saucedo-Muñoz, M.L.; Torres Castillo, A.A. β′ phase decomposition in Zn-22 mass% Al and Zn-22 mass% Al-2 mass% Cu alloys at room temperature. *Mater. Trans.* **2007**, *48*, 2791–2794. [CrossRef]
24. Wang, Y.; Zeng, J. Eutectoid transformation in Zn alloy with high Al content. *Adv. Mater. Res.* **2013**, *652*, 1111–1114. [CrossRef]

25. Arif, M.A.M.; Omar Muhamad, M.Z.; Syarif, J.; Kapranos, P. Microstructural evolution of solid-solution-treated Zn-22Al in the semisolid state. *J. Mater. Sci. Technol.* **2013**, *29*, 765–780. [CrossRef]
26. Arif, M.A.M.; Omar, M.Z.; Muhamad, N. Effect of solid solution treatment on semisolid microstructure of Zn-22Al alloy. *J. Sci. Technol.* **2012**, *21*, 121–126.
27. Liu, Y.; Li, H.; Jiang, H.; Lu, X. Effects of heat treatment on microstructure and mechanical properties of ZA27 alloy. *Trans. Nonferrous Met. Soc. China* **2013**, *23*, 642–649. [CrossRef]
28. Agapie, M.; Peter, I.; Varga, B. Structure of cooled Zn–Al eutectoid based alloys in biphasic domain. *J. Optoelectron. Adv. Mater.* **2015**, *17*, 1842–1848.